Studies of Nuclear Effects and Charge Symmetry Violation using a Deuterium Target in MINERνA

The MINERνA Collaboration

(Dated: May 14, 2011)

Abstract

Neutrino scattering provides a powerful experimental tool for studying the basic structure of protons and neutrons in terms of both the parton distributions functions (PDFs) of deep inelastic scattering and the form factors of elastic scattering. While scattering with charged lepton beams cannot distinguish between quark flavors, neutrino and anti-neutrino scattering can separate individual quark flavors and quarks from anti-quarks. While this has been recognized for many years, the full power of neutrino scattering has not yet been fully realized. Most neutrino scattering experiments have been performed on heavy nuclei in order to increase the interaction rates and provide adequate statistical precision, and the utilization of such data in determining PDFs from global fits has been hampered by the possibly large and unknown nuclear effects in neutrino scattering (sections II.1 and II.2). While significant progress has been made in producing high intensity, energy-selected neutrino beams, as well as methods for both the monitoring and determination of the beam flux, essentially no new experiments have been performed on deuterium or hydrogen targets in nearly 25 years. The availability of the high intensity NuMI beam at Fermilab provides a unique opportunity to address fundamental questions concerning the quark structure of the nucleon and to unravel the physics underlying the nuclear dependence of neutrino scattering.

We propose to fill the existing MINERνA cryogenic target with liquid deuterium to take advantage of this opportunity. The high intensity neutrino and anti-neutrino beams from the Fermilab NuMI facility, especially after upgrades for NOνA and the addition of deuterium to the existing MINERνA targets of carbon, iron, lead, water, scintillator and the aluminum of the cryostat, allow for the highest precision nuclear to deuterium ratio (A/D) measurements via flavor sensitive weak interactions with a range of different atomic numbers and nuclear densities. The expected statistics from this data could provide ratios of iron to deuterium structure functions at the 3% uncertainty from $0.05 < x < 0.6$ in neutrino/antineutrino mode (section IV.1), and the ability to see charge symmetry violation at the 3% level in the same x range (section IV.2). The physics payoff for this effort is the inclusion of neutrino constraints on sea and low-x valence quarks in the nucleon to the global PDF fits, and an independent measure of charge-symmetry violations in parton distributions, which may be the source of the difference between the Weinberg angle measured by the NuTeV collaboration and the standard model prediction.

CONTENTS

I. INTRODUCTION

Over the past three decades following the original European Muon Collaboration (EMC) observation, experiments at CERN and SLAC have firmly established that structure functions in nuclei differ significantly from those in free nucleons. The nucleus cannot be simply described as a collection of on-shell nucleons. The nucleon averaged structure function F_2^A deviates from F_2^D as a function of Bjorken x. Figure 1 shows as an example the ratio of the inclusive deep-inelastic cross section on iron to that of deuterium as measured by the EMC collaboration [1]. The corresponding deviation of the structure function ratio, F_2^A/F_2^D, from unity shows a clear dependence on Bjorken x, and is generally separated into four regions, each depending on a different physics mechanism: the shadowing region with $0 < x < 0.1$, the anti-shadowing region with $0.1 < x < 0.3$, the nuclear "EMC effect" region with $0.3 < x < 0.7$, and the Fermi motion region with $x > 0.7$.

In spite of a large body of experimental and theoretical efforts, the underlying mechanisms for the regions in x below the rise due to Fermi motion is still not commonly accepted. A simple fit to the EMC region data as a function of atomic mass does not work well for light nuclei and the A=4 helium behaves similarly to the A=12 carbon in the nuclear EMC effect region [2]. The A/D ratios in Drell-Yan data, without any obvious anti-shadowing effect, show a different x-dependence from those with charged lepton beams [3]. The A/D ratios from neutrino and anti-neutrino beams, in terms of Ne/D [5], seem to be compatible with the charged lepton data; however, the precision does not allow for a firm statement to be made.

A precise understanding of the nuclear effects becomes very important for nuclear neutrino data with high statistics, for example the NuTeV data on an iron target [6]. The nuclear correction might be the key to reducing the conflict between the NuTeV data and the E866 Drell-Yan data in the global fit of PDFs (Parton Distribution Functions) [7]. In addition, the nuclear corrections in neutrino scattering, obtained by comparing the iron structure functions from NuTeV data and the global free-proton PDF fit, appear to differ in both shape and magnitude from those in models and charged lepton data [8].

We propose to include a liquid deuterium target in the MINERvA experiment for the purpose of comparing the differential cross sections from the nuclear targets to those from the simplest isoscalar target, deuterium. This will allow for the highest precision measure-

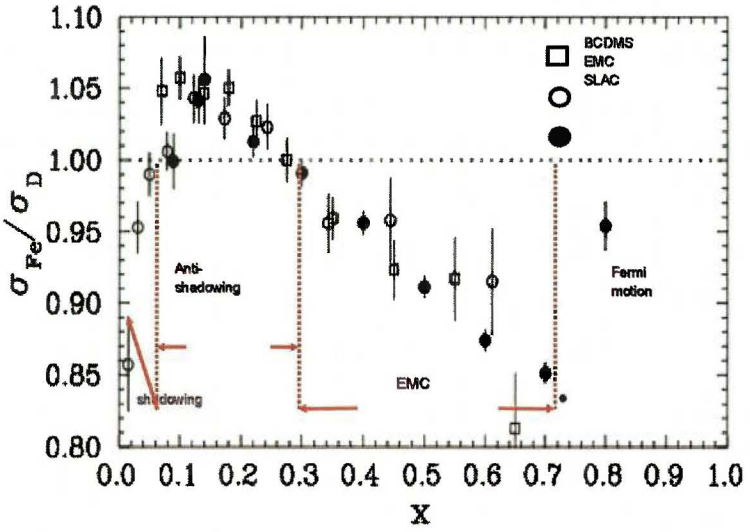

FIG. 1. [1] Iron to deuterium cross section ratio σ_{Fe}/σ_D as a function of x from EMC (open circles), SLAC (solid circles) and BCDMS (open squares). The data has been averaged over Q^2 and corrected for neutron excess.

ments to date of these ratios via flavor sensitive weak interactions, and will allow several fundamental physics questions to be addressed. First, these ratios will provide the best possible sensitivity for probing differences in the nuclear medium modifications between the structure functions for neutrino and charged-lepton scattering [8]. Understanding possible differences will be critical input required for including the nuclear neutrino data in the global fits to constrain the nucleon PDFs, which will benefit the luminosity measurement at LHC. Second, ratios of neutrino and anti-neutrino cross sections from the deuterium provide direct sensitivity to possible charge symmetry violation (CSV) effects at the quark level. While quite interesting in their own right, the observation of CSV effects could have a profound impact on both predicted standard model physics at the Tevatron and LHC stemming from the input of PDF fits, as well as the interpretation of the NuTeV measurement of the Weinberg angle. Third, charged-current quasi-elastic (QEL) scattering from the neutron in the deuterium will provide a significant baseline measurement for the medium modification of the axial form factors, which would aid in the interpretation of long baseline neutrino oscillation experiments.

The NuMI facility at Fermilab provides the highest intensity neutrino and anti-neutrino

beams currently available, which makes it possible to perform measurements with light targets like deuterium and hydrogen with good statistical precision. In addition, the current MINERνA cryogenic target has been designed to store both liquid deuterium and hydrogen in addition to helium, although it will requires extra safety measures not currently in place.

In this Letter of Intent, we discuss the physics and the expected impact of the proposed deuterium data based on the MINERνA's detector simulation and guided by MINERνA's current analysis techniques and our understanding of detector performance. In the appendix, we will discuss the physics potential of filling the MINERνA cryogenic target with hydrogen.

II. PHYSICS MOTIVATION

II.1. Determining the Quark Content of Nucleon Structure Functions: PDFs

The weak interaction provides a powerful probe to separate both the flavor and the valence/sea dependence of the PDFs. In this section we will illustrate this by use of the Leading Order (LO) approximation provided by the quark-parton model. However, we stress that the full power of such measurements will only be realized once the results are incorporated into global PDF fits.

The inclusive differential cross sections per nucleon for neutrino and anti-neutrino charged current DIS scattering $\nu(\bar{\nu})+p \rightarrow \mu^-(\mu^+)+X$ can be defined by three dimensionless structure functions $F_i^{\nu(\bar{\nu})}, i = 1,2,3$ [9, 10]:

$$\frac{d^2\sigma^{\nu(\bar{\nu})}}{dxdy} = \frac{G_F^2 M_p E_{\nu(\bar{\nu})}}{\pi}\left(\frac{M_W^2}{M_W^2+Q^2}\right)^2\Big[xy^2F_1^{\nu(\bar{\nu})}(x,Q^2) + (1-y-\frac{M_p xy}{2E_{\nu(\bar{\nu})}})F_2^{\nu(\bar{\nu})}(x,Q^2) \pm y(1-\frac{y}{2})xF_3^{\nu(\bar{\nu})}(x,Q^2)\Big] \quad , \tag{1}$$

where $E_{\nu(\bar{\nu})}$ is the neutrino or anti-neutrino beam energy (corresponding to the upper or lower sign), Q^2 is the square of the four-momentum transfer, $y = \frac{\nu}{E_\nu}$ is the ratio of the hadronic energy $\nu = E_\nu - E_\mu$ to the neutrino beam energy, M_p is the proton mass, Bjorken $x = \frac{Q^2}{2M_p\nu}$ is the momentum fraction carried by the quarks, and G_F is the Fermi coupling constant. The structure functions F_1 and F_2 are related to the cross section ratio $R = \sigma_L/\sigma_T$ between scattering via longitudinal to transversely polarized W bosons:

$$2xF_1 = F_2\frac{1+4M^2x^2/Q^2}{1+R} \quad . \tag{2}$$

At Q^2 much smaller than the W mass, the above equation reduces to

$$\frac{d^2\sigma^{\nu(\bar{\nu})}}{dxdy} = \frac{G_F^2 M_p E_{\nu(\bar{\nu})}}{\pi}\left[\left(1-y(1+\frac{M_p x}{2E_{\nu(\bar{\nu})}})+y^2\frac{1+4M^2x^2/Q^2}{1+R}\right)F_2^{\nu(\bar{\nu})}(x,Q^2)\right.$$
$$\left.\pm\left(y-\frac{y^2}{2}\right)xF_3^{\nu(\bar{\nu})}(x,Q^2)\right]. \tag{3}$$

In the leading-order parton model with $m_p << E_\nu$ and $m_N << Q << M_W$, $F_2 \sim 2xF_1$ and the structure functions are related to the parton distribution functions by

$$F_1^{\nu p} = d(x) + s(x) + \bar{u}(x) + \bar{c}(x) \sim \frac{F_2^{\nu p}}{2x} \tag{4a}$$
$$F_1^{\bar{\nu}p} = u(x) + c(x) + \bar{d}(x) + \bar{s}(x) \sim \frac{F_2^{\bar{\nu}p}}{2x} \tag{4b}$$
$$F_3^{\nu p} = 2\left[d(x) + s(x) - \bar{u}(x) - \bar{c}(x)\right] \tag{4c}$$
$$F_3^{\bar{\nu}p} = 2\left[u(x) + c(x) - \bar{d}(x) - \bar{s}(x)\right] \tag{4d}$$

Therefore the inclusive differential cross sections for neutrino and anti-neutrino charged current scattering on deuterium target with any small nuclear effects from the barely bound deuterium, can be expressed as:

$$\frac{d^2\sigma^{\nu(p+n)}}{dxdy} \approx \frac{G_F^2 M_p E_\nu}{\pi}\cdot 2x\left[(d_{p+n}+s_{p+n})+(1-y)^2(\bar{u}_{p+n}+\bar{c}_{p+n})\right] \tag{5a}$$
$$\frac{d^2\sigma^{\bar{\nu}(p+n)}}{dxdy} \approx \frac{G_F^2 M_p E_\nu}{\pi}\cdot 2x\left[(1-y)^2(u_{p+n}+c_{p+n})+(\bar{d}_{p+n}+\bar{s}_{p+n})\right] \tag{5b}$$

We can form the neutrino to anti-neutrino cross section ratio,

$$\frac{\frac{d^2\sigma^{\nu D}}{dxdy}}{\frac{d^2\sigma^{\bar{\nu}D}}{dxdy}} \approx \frac{d_p(x)+d_n(x)}{u_p(x)+u_n(x)}\cdot\frac{1}{(1-y)^2}. \tag{6}$$

Under the assumption of charge symmetry, $d_p = u_n$ and $d_n = u_p$, Eqn. 6 becomes

$$\frac{d^2\sigma^{\nu D}}{d^2\sigma^{\bar{\nu}D}} \sim \frac{1}{(1-y)^2}. \tag{7}$$

Any deviation from this relation is strong evidence of charge symmetry violation at the quark level.

II.2. Nuclear Medium Modifications of Nucleon Structure

II.2.1. The Nuclear EMC Effect

The EMC effect [1] has been well measured with charged lepton beams. It describes the suppression of the average nucleon F_2^A structure function relative to deuterium in the region of $0.3 < x < 0.7$. In this x region, the F_2^A/F_2^D ratio, which is approximately proportional to the DIS cross section ratio σ^A/σ^D, is less than 1 and decreases linearly with increasing x. There is no unique theory or universally accepted model that can describe its origin, despite the intense theoretical work since its discovery in 1983. The shape of the x dependence of the EMC effect is similar for different nuclei. The magnitude of the EMC effect at $x = 0.6$ was plotted as a function of atomic number A and the average nuclear density ρ, as seen in Figure 2 [11]. With the nuclear density estimated assuming a uniform sphere with the RMS charge radius from electron scattering. This yields a nuclear density for Helium which is very similar to that of carbon. The recent JLab E03-013 data [2] showed that the EMC effect for ^4He is similar to that for ^{12}C, as shown in Figure 3 [12]. This suggests that the EMC effect does not solely depend on the atomic number A. This can be also shown quantitatively as the slope of A/D ratio in the EMC region, as seen in Figure 4 [2]. This figure also indicates that the EMC effect for ^9Be does not follow the density-dependence fit [2].

The JLab E03-013 data [12], as shown in Figure 3, indicate that the scaling of the nuclear structure functions observed in the DIS regime ($W > 2$) extends to W values in the resonance region. The high x part of the EMC data, with W down to $\sqrt{2}$, show a smooth continuation with the low x part of the data with $W > 2$.

II.2.2. Nuclear Effects for Neutrino Scattering

In contrast to nuclear effects in charged lepton scattering, the nuclear effects in neutrino scattering have not been directly measured and are not well constrained by global fits. A better knowledge of the nuclear effects is crucial to use the nuclear neutrino data to constrain the nucleon PDFs. For example, the neutrino data on iron from the NuTeV experiment, corrected to free nucleon with the Kulagin-Petti model, favors a different d/u ratio than that of the Drell-Yan data from Fermilab E866 experiment at large x [7]. When fitting simultaneously, as shown in Figure 5 [7], this tension between E866 and NuTeV causes an

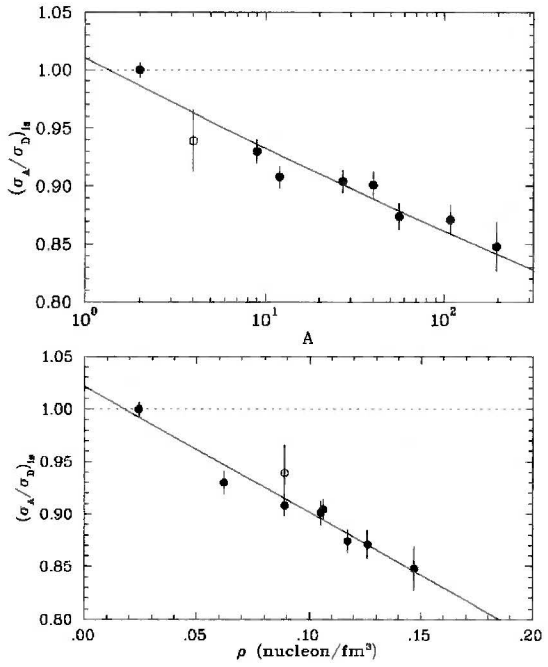

FIG. 2. [11] σ^A/σ^D ratio at x=0.6 from SLAC E139 experiment plotted as a function of mass number and nuclear density. The data are averaged over all Q^2 and corrected for neutron excess. Errors include statistical uncertainties, point-to-point and target-to-target systematic uncertainties. The open circle is the SLAC data for ^4He. The solid circle at the same density is for ^{12}C. The fitting functions are $[\sigma^A/\sigma^D](A) = C(x)A^{\alpha(x)}$ and $[\sigma^A/\sigma^D](\rho) = D(x)[1 + \beta(x)\rho]$.

obvious change in the d/u ratio at large x and a significant increase in the χ^2 of the overall fit.

The conflict between NuTeV and E866 could be reduced by adjusting the nuclear corrections. In addition, the nuclear corrections, obtained by comparing the iron PDFs extracted directly from NuTeV data and the free-nucleon PDFs from the global parameterization, differ in both shape and magnitude from those in the models and charged lepton data, as shown in Figure 6 [8]. The Kulagin-Petti model is consistent with the SLAC/NMC data with charged lepton beams with anti-shadowing around $0.06 < x < 0.3$ and EMC effect around $0.3 < x < 0.7$. However the fit of the NuTeV iron data seems to suggest a smaller anti-shadowing effect and in a much lower x region, around $0.01 < x < 0.08$, and is more consistent with Fermilab E772 Drell-Yan data which did not show a very clear anti-shadowing

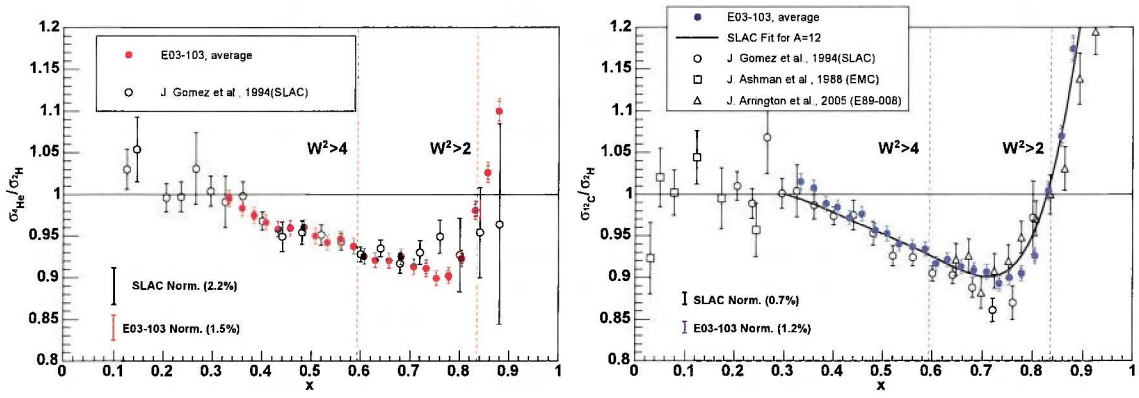

FIG. 3. [12] Preliminary EMC ratios from JLab E03-103 for the ^4He and ^{12}C (in solid circles), as well as the existing A/D ratios (in open symbols). The inner error bars are statistical, while the outer error bars are the combined statistical and estimated systematic uncertainty.

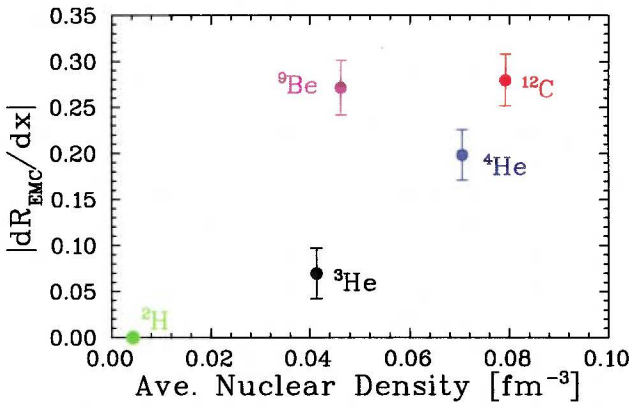

FIG. 4. [2] The slope of the isoscalar EMC ratio for $0.35 < x < 0.7$ as a function of nuclear density. Error bars include statistical and systematic uncertainties. Note that deuterium is observed to be almost free of nuclear effects and has a very low nuclear density compared to other targets to be studied in MINERνA.

effect [3]. It is important to check whether this effect persists in neutrino scattering from other nuclei and whether the A/D ratios may be different between the parity violating structure function F_3 and F_2, especially at low x and low Q^2 [13].

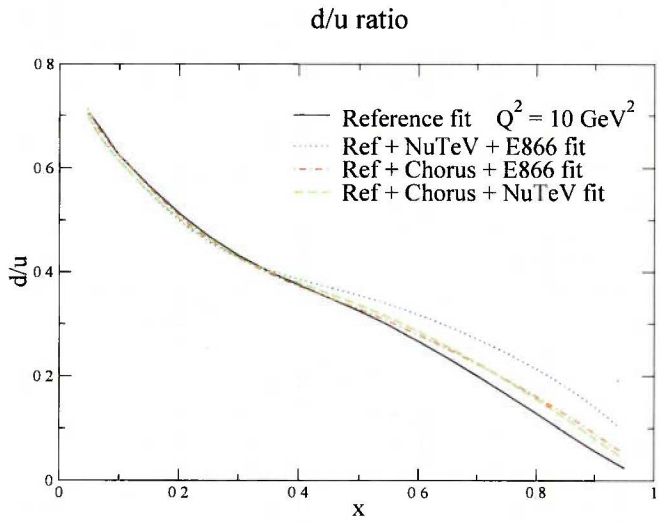

FIG. 5. [7] Comparisons of the d/u ratios from the reference fit and three additional fits with different combinations of new data sets. The change of d/u ratio is bigger and the χ^2 is worse if adding E866 and NuTeV data together to the reference fit.

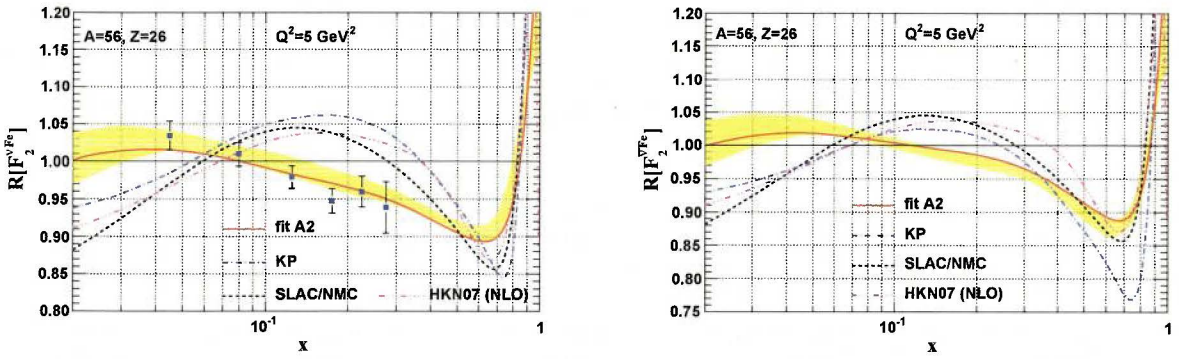

FIG. 6. [8] The nuclear correction factor, F_2^{Fe}/F_2^D, was plotted as a function of Bjorken x for neutrino (left panel) and anti-neutrino beam (right panel). The A2 fit (solid red line) was obtained by taking the ratio of the NuTeV iron data (blue solid squares) to the CTEQ free proton PDFs. The yellow error band represents the fit uncertainties. The fit results were compared with the SLAC/NMC parameterization (dashed line), the Kulagin-Petti model prediction for neutrino scattering (dashed-dot line) and HKN07 nuclear PDF fits (dashed-dotted line) for charged lepton scattering.

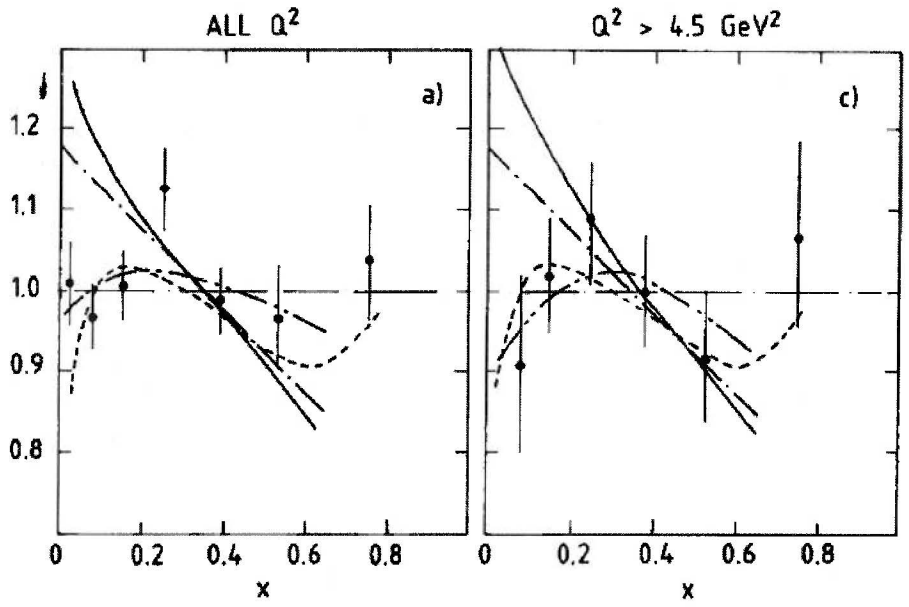

FIG. 7. [4] The nucleon averaged $\bar{\nu}Ne$ to $\bar{\nu}D_2$ cross section ratios from BEBC as a function of Bjorken x. The error bars include both statistical and systematic errors. The overlaid lines are the SLAC (dashed), EMC(dashed-dot) and QPM (solid) model predictions, as well as the QPM (dashed-double-dot) predictions with the best fit parameters.

II.2.3. Existing A/D Ratio with Neutrino and Anti-neutrino Beams

The BEBC collaboration used neutrino and anti-neutrino interactions in a bubble chamber to compare the differential cross sections per nucleon in neon (WA59) and those in deuterium (WA25) [5]. The anti-neutrino Ne/D ratios were compared with those from EMC muon and SLAC electron data using various models. Overall, the anti-neutrino data appears to be compatible with the charged lepton data, as seen in Figure 7 [4], but the statistical precision with this single target ratio is not sufficient to draw any firm conclusions.

II.3. Charge Symmetry Violation at the Quark Level

Charge symmetry, i.e. $u_p = d_n; d_p = u_n$, is an important *assumption* in the current global parameterizations of the PDFs. It is a more restrictive symmetry than isospin symmetry and is generally obeyed at the level of a fraction of 1% for static properties of the nucleon.

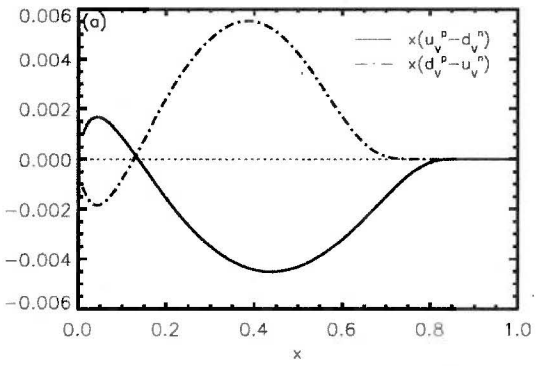

FIG. 8. The valence quark CSV from MIT bag model (solid curve for $x\delta u_v$ and dashed for $x\delta d_v$)[20].

However charge symmetry has never been tested with precision at the quark level. The upper limit on the magnitude of the CSV (Charge Symmetry Violation) is 6-9% in the region of $0.1 < x < 0.4$ based on the comparison between the neutrino CCFR and lepton NMC DIS data on isoscalar targets [14]. Sizable CSV, even at a level consistent with this limit, would modify the way to combine the neutron and proton data and affect the extraction of the fundamental PDFs. For example, the light flavor asymmetry ($\bar{d} - \bar{u} \neq 0$) might not exist or should be modified if there is sizable CSV in the sea quark or valence quark distributions. The violation of the Gottfried integral based on NMC data could be due to light flavor asymmetry in the proton sea, or due to CSV of more than 8% for the sea quarks, or a combination of both effects [16, 17]. The other light flavor measurements, NA51 and E866 Drell-Yan and HERMES semi-inclusive DIS data, are all subject to charge symmetry correction due to the usage of deuterium target. Finally, the NuTeV anomaly could be explained partially or completely by the charge symmetry violation in valence quark distributions at the quark level [18, 19].

Theoretical investigations of CSV have been carried out in a quark model [18] and in the MIT bag model [20]. MRST has tried to extract constraints on CSV in their global fit [21] by assuming a particular functional form, $\delta u_v(x) = -\delta d_v(x) = \kappa f(x)$ with $f(x) = (1-x)^4 x^{-0.5}(x - 0.0909)$. Their best fit value of κ is -0.2, which is similar to the effect predicted in models; however, within 90% confidence their fit allows $-0.8 \leq \kappa \leq +0.65$, so there is little sensitivity.

A JLab 12 GeV upgrade proposal, E09-002 [22], plans to measure the CSV in the valence

quark distribution in terms of $\frac{-4(\delta d-\delta u)}{3(u_v+d_v)}$ via the π^+/π^- production ratios in semi-inclusive DIS.

III. MINERνA EXPERIMENT WITH A DEUTERIUM TARGET

III.1. The NuMI Neutrino Beam

The Fermilab NuMI (Neutrinos at the Main Injector) beam line begins with the Main Injector accelerator delivering 120 GeV protons to a graphite target producing secondary pions and kaons. It is expected that the Main Injector will deliver $\sim 6 \times 10^{20}$ POT (protons on target) per year after the NOνA [24] beam line upgrade bringing the beam power from 350 kW to 700 kW.

The neutrino beam energy is a strong function of the the relative target and horn positions in the NuMI beamline. The MINOS experiment [25] uses a Low Energy (LE) configuration, which is best suited for the study of the neutrino oscillations with a far detector on the beam-line axis. The NOνA experiment [24] will use the Medium Energy (ME) configuration since it is optimum for the study of neutrino oscillations with an off-axis detector. MINERνA [9], with its on-axis detector upstream of the MINOS near detector, can run together with both the MINOS and NOνA experiments. We propose to add the deuterium target when NOνA is starting to run, and therefore we will focus on ν-D scattering using the NOνA ME fluxes. NOνA plans to run 3 years of neutrino and 3 years of anti-neutrino beam.

III.2. MINERνA Deuterium Target Statistics

The statistics of Charged-Current (CC) events produced on the 0.37 ton cryogenic deuterium target with the NOνA ME muon neutrino flux can be estimated by using the GENIE [26] neutrino event generator. We will focus on the CC events from ν_μ ($\bar{\nu}_\mu$), which is the dominant flavor in the ME neutrino (anti-neutrino) beam. The x versus Q^2 distribution of the CC events is shown in Figure 9. The Quasi-Elastic (QEL) events feature a peak in W at the proton mass W=0.938 GeV ($x = 1$), corresponding to the process $\nu_\mu n \rightarrow \mu p$. The events with a W greater than 2 GeV correspond to the charm process. The resonance (RES) events have a clear peak around the Δ mass (1.232 GeV). There is no clear resonance

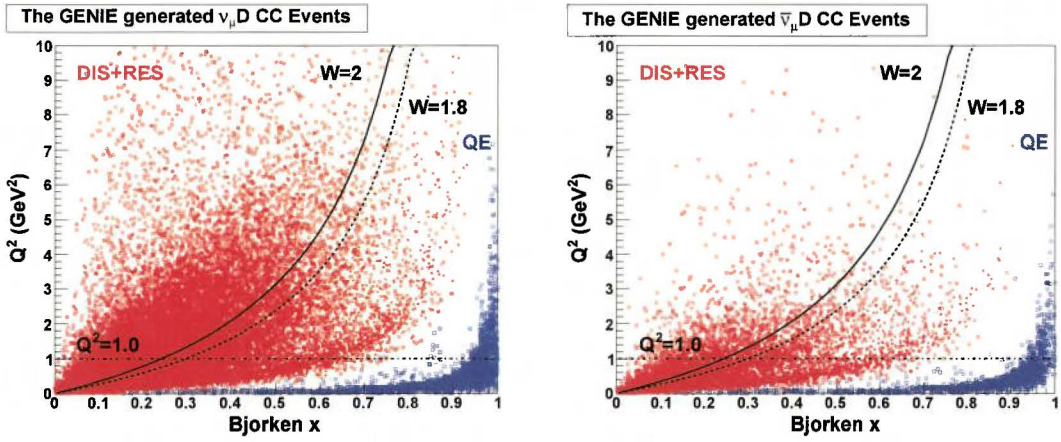

FIG. 9. $x - Q^2$ generation phase space for events from the cryogenic deuterium target based on the NOνA neutrino (left) and anti-neutrino (right) ME flux, and utilizing the GENIE Monte Carlo generator. CC-QEL events are indicated in blue.

structure above $W > 1.8$ GeV. The DIS process dominates the muon CC events at the large neutrino energy and large invariant mass.

III.3. Acceptance Studies

The MINOS near detector, located just downstream of the MINERνA detector, is a steel-scintillator tracking calorimeter with a 1.3 T toroidal magnetic field. The steel plates are 2.54 cm thick and the scintillator planes are comprised of 4.1 cm wide and 1 cm thick plastic strips. Some muons exit the MINERνA detector and enter the MINOS near detector. The momentum and charge of these muons can be determined by the MINOS near detector, based on their ranges and track curvatures in the magnetic field, respectively. MINERνA is already successfully reconstructing events with muons that enter into the MINOS near detector using MINOS Near Detector data. The MINERνA collaboration has also shown excellent momentum determination as well as particle identification for muons and hadrons, based on the ionization energy loss patterns and ranges in the MINERνA detector. The momentum of the muon can be accuratley determined by range if it stops in the ID (Inner Detector) of MINERνA (ID contained track). The reconstruction of muon momenta for the OD (Outer Detector) contained tracks is less precise due to more coarse detector segmentation. For events from the passive cryogenic target upstream of the MINERνA detector, a muon plus

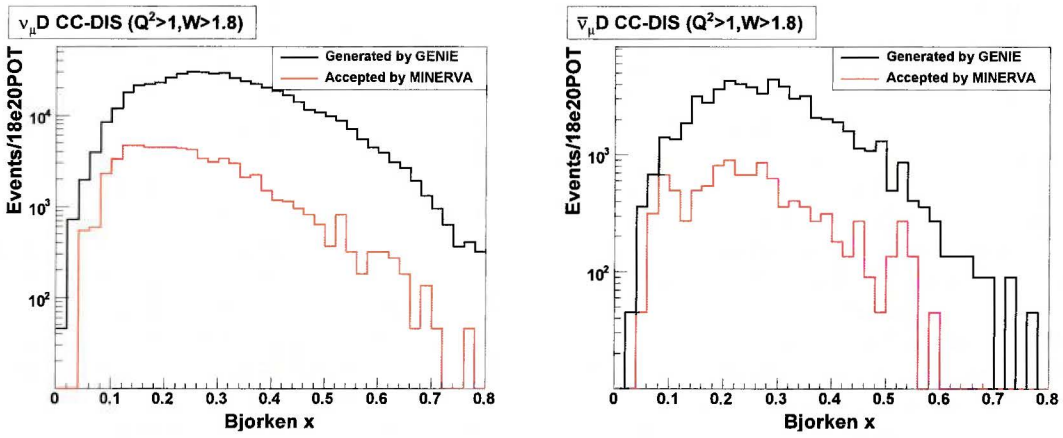

FIG. 10. CC-DIS statistics with different acceptance cuts for 3-year (18e20 POT) NOνA neutrino (left) and anti-neutrino (right) ME beam on deuterium target, as a function of Bjorken x.

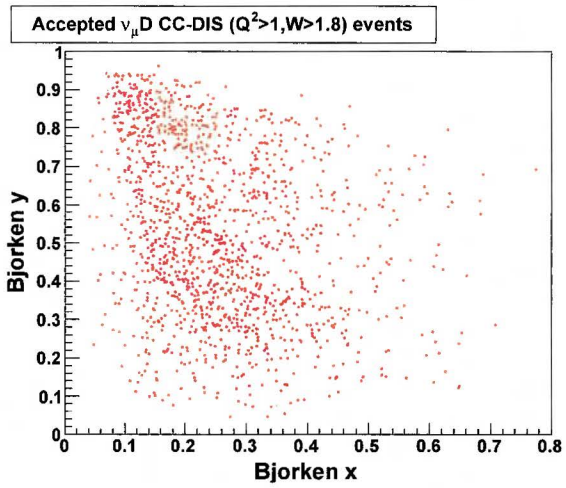

FIG. 11. y vs x acceptance coverage for CC-DIS events for 3-year (18e20 POT) NOνA ME neutrino beam on deuterium target. Coverage for the anti-neutrino beam is similar.

another track in the MINERνA detector are required to reconstruct the interaction vertex. The loss of acceptance from the requirement of a reconstructable muon and this second track is significant and is included in the sensitivity projections in this Letter.

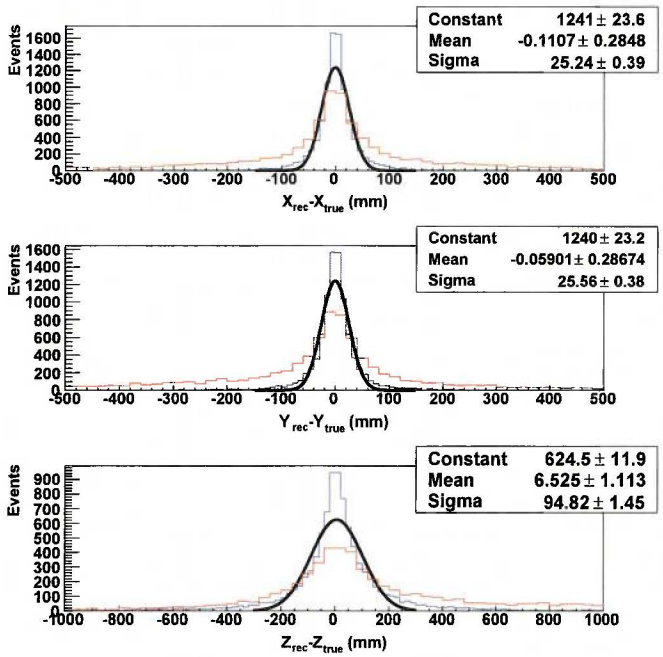

FIG. 12. The residuals of the neutrino event vertex distributions, defined as the difference between the reconstructed and true vertices along each detector axis in millimeters, for muon CC events on a deuterium target with the NOνA ME flux. Red curves show the reconstruction status for two-track events with MINERνA simulation package available at the time of this writing. The blue curves are obtained with Monte-Carlo assisted tracking, which uses true particle ID to sort the digitized hits and reflect the future goals. The black curves are fitting the blue curves.

III.4. Vertex Reconstruction: Target Vessel Background Elimination

The correspondence between the two-track reconstructed vertices and true vertices is shown in Figure 12. The vertex reconstruction is the worst in z direction (along the beam axis) because the tracks are boosted forward in z. Because the vertex reconstruction is not perfect, the selection cut identifying the event as coming from the cryogenic volume will not remove all background from interactions in the aluminum cryostat. To address this, we plan to spend some running time with an empty target, and this run time on the empty target is optimized based on the ratio of the yields of deuterium events to aluminum wall events. The loss of beam time on the empty target and the background subtraction results in an increase in projected statistical uncertainties for deuterium scattering results by 47%

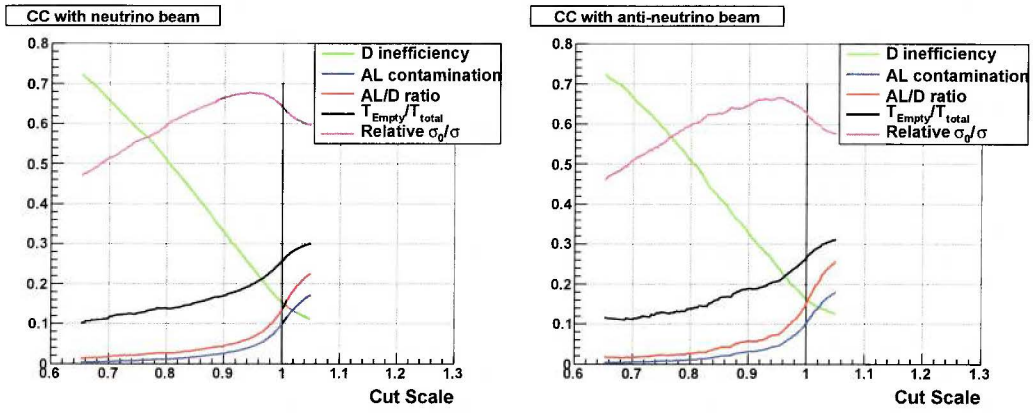

FIG. 13. The empty target optimization for deuterium target with NOνA neutrino (left) and anti-neutrino (right) ME flux, as a function of the cut scale. The vertex cut is a three-dimensional shape close to that of the inner cryogenic vessel. The scale factor refers to the scale in length. The σ_0 refers to the raw relative statistical uncertainty, which is smaller than the real relative statistical uncertainty σ suffering empty target subtraction. Also plotted are the inefficiency in deuterium events, the contamination from the background aluminum, the aluminum to deuterium ratio, the optimized empty running to total beam time.

for the neutrino beam and 50% for anti-neutrino beam. In the remainder of this document this effect on the statistical uncertainties is included in our projections.

III.5. A Possible MINERνA Detector Upgrade

The position resolution of the hits in the Inner Detector of MINERνA is excellent and being put to good use in current MINERνA analyses. However the reconstruction is much more difficult for the outer detector (OD) due to coarse resolution and significant passive material. This particularly affects the cryogenic target events because the cryogenic target is spatially large and wide angle tracks often will first appear in the outer detector. To improve the acceptance of such high Q^2 events, especially QEL, we are studying a modest upgrade to add larger scintillators planes, roughly the size of the OD, to increase the angular acceptance and improve track reconstruction. The required area of scintillator plane is only a few percent of the total MINERνA inner detector some spares from MINERνA production may be usable for this detector.

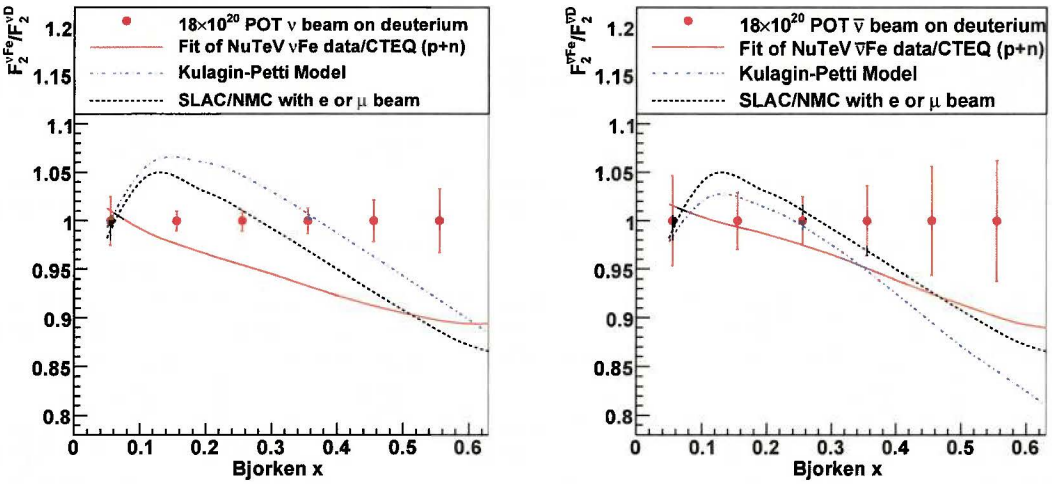

FIG. 14. The statistical errors in MINERνA's projected Fe/D ratio based on the DIS simulation, with the NOνA neutrino (left) and anti-neutrino (right) ME beams. The curves were read from reference [8]: The red solid line was obtained by comparing the nuclear PDFs extracted from the NuTeV iron data and the CTEQ free-nucleon PDFs, while the blue dashed-dot line was from the Kulagin-Petti model, and the black dashed line was a fit of the SLAC/NMC data with charged lepton beam.

IV. PROPOSED MEASUREMENTS ON DEUTERIUM

IV.1. x-dependent Nuclear Effects

The NuTeV iron data suggests different nuclear dependence from what was predicted by the existing models and observed in charged lepton data. The MINERνA experiment will measure the DIS cross section on a variety of material: carbon, iron and lead, water and scintillator, as well as aluminum in the cryostat. By adding deuterium to the suite of target materials, MINERνA can measure F_2^A/F_2^D ratios from the neutrino and anti-neutrino beams directly and compare them to those from charged lepton scattering. The projected statistical uncertainties with NOνA medium energy flux are shown in Figure 14 in terms of the Fe/D ratio. The statistical uncertainties shown are dominated by the deuterium target which has the lowest statistics of any target, except the aluminum of the cryostat, by

a large factor. In both the neutrino and anti-neutrino beams, the ratios can be measured as a function of x to better than 5% for the expected run of 3 years each of neutrino and antineutrino beams with 6×10^{20} protons on target per year.

IV.2. Sensitivity to Charge Symmetry Violations

Recall from Eqn. 6 that there is a definite prediction for the ratio of neutrino to anti-neutrino cross-sections on deuterium if charge symmetry holds. We propose to measure charge symmetry violation by looking for deviations from this prediction.

To show the sensitivity to a particular charge symmetry violation model, we make the assumption that $u_p - d_n = -(d_p - u_n) \equiv \delta(x)$. Then,

$$1 - (1-y)^2 \frac{\frac{d^2\sigma^{\nu D}}{dxdy}}{\frac{d^2\sigma^{\bar{\nu} D}}{dxdy}} \approx 2\delta(x)/[u(x) + d(x)]. \tag{8}$$

Figure 15 shows that running with deuterium would provide a measurement or constraint at better than five per cent for $0.05 < x < .45$.

V. CONCLUSIONS

With the high neutrino and anti-neutrino fluxes provided by the NuMI beam line in the NOνA era, it is possible to carry out statistically significant measurements on a 0.37 ton deuterium target. The systematics associated with these measurements are expected to be reduced compared to previous neutrino experiments due to the ability to take data simultaneously on several different nuclei, and the fact that the NuMI beamline neutrino production will have been measured using a variety of techniques. Combined with data from the MINERνA nuclear targets of Pb, Fe, C, water, plastic scintillator, and Al from the cryotarget vessel, measurements of neutrino scattering on deuterium will greatly improve our knowledge in the medium modifications of nucleon structure, as well as find or put few per cent limits on charge symmetry violation in the nucleon.

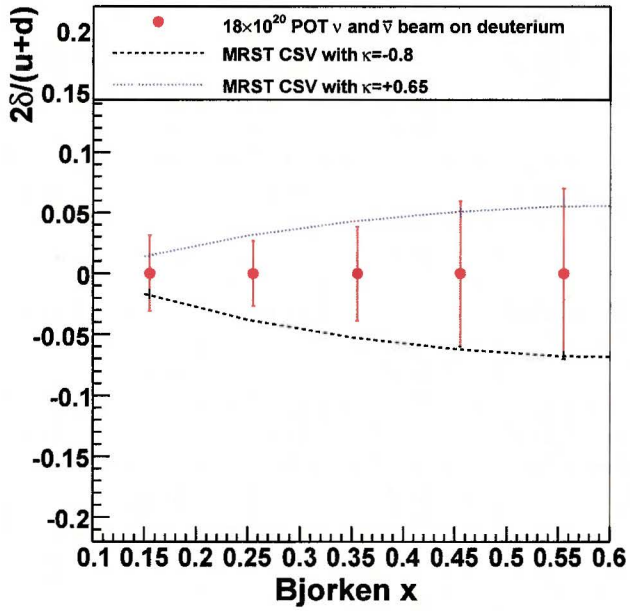

FIG. 15. MINERνA's projected sensitivity to the charge symmetry violation with a deuterium target in terms of $2(u_p - d_n)/(u_p + d_p) \equiv 2\delta/(u_p + d_p)$ as a function of Bjorken x. The 90% confidence level range in this parameter for CSV from MRST is also shown, although it is important to recall that this limit assumes a particular shape of the CSV effect in x and that CSV appears in particular quark distributions. The MINERνA sensitivity to CSV is more general.

Appendix A: Hydrogen Target for MINERνA

The main focus of this document has been the physics reach gained by adding deuterium as a target to MINERνA. However the MINERνA cryogenic target could also be filled with hydrogen. The technical requirements for hydrogen are essentially the same as those for deuterium. The physics case for hydrogen, however, is significantly different than that for deuterium.

With the beginning of operations at LHC, precision knowledge of PDFs is increasingly important to measurements from the evaluation of sensitivity to new discoveries to precise knowledge of luminosities from "standard candle" processes, like W and Z production. A major challenge of the extraction of PDFs is the flavor decomposition, i.e. how to separate the contribution from gluons and different types of quarks and anti-quarks. The precise

DIS data with charged lepton beams (including electron and muon) is sensitive to the same combination of the parton distributions, i.e. the charge square weighted sum of all partons $\sum_q e_q^2 q$. The gluon contribution is determined mainly through the Q^2 evolution of the structure functions. There are six pairs of quark and anti-quark flavors in total, but the large x region where the sea quark and anti-quarks can be ignored, is dominated by the up u and down d quarks only. However, hydrogen target data alone is not enough to decompose the u and d distributions from charged lepton scattering, since it is not sensitive to flavor. Decomposition using neutrons from deuterium requires the assumption of charge symmetry, and similar decomposition using neutrino data on heavy targets requires knowledge of nuclear corrections. However, as previously discussed, the nuclear effects are not well understood even in the well-studied nuclear to deuterium (A/D) ratios from charged lepton scattering, and these effects could be both different and larger in the case of neutrino scattering.

There are proposals to control nuclear effects in the determinations of neutron structure, for example there are two JLab 12 GeV proposals to measure d/u ratio at $x \to 1$. Pne of these is the BONUS12 experiment [30], which extends the existing 6 GeV measurements of F_2n/F_2^p to 12 GeV and minimizes the nuclear effects by controlling the kinematics with spectator tagging technique. Another is the MARATHON experiment [31], which uses the isobar A=3 targets (helium and tritium) to largely cancel the nuclear effects. However, both of these experiments rely on the assumption of small or vanishing CSV to extract information on d/u. Alternatively, DIS scattering on a hydrogen target with both neutrino and anti-neutrino beams can measure d/u free of both nuclear effects and the assumption of charge symmetry. In the large x region where the sea quark distribution can be ignored, the inclusive differential cross section can be simplified to

$$\frac{d^2\sigma^{\nu p}}{dxdy} \sim \frac{G_F^2 M_p E_\nu}{\pi} 2xd(x) \tag{A1a}$$

$$\frac{d^2\sigma^{\bar{\nu} p}}{dxdy} \sim \frac{G_F^2 M_p E_\nu}{\pi} 2x(1-y)^2 u(x)\ , \tag{A1b}$$

which implies that the neutrino to anti-neutrino cross section ratio is proportional to d/u ratio at large x for a hydrogen target:

$$\frac{d}{u} \sim (1-y)^2 \frac{d^2\sigma^{\nu p}}{d^2\sigma^{\bar{\nu} p}}. \tag{A2}$$

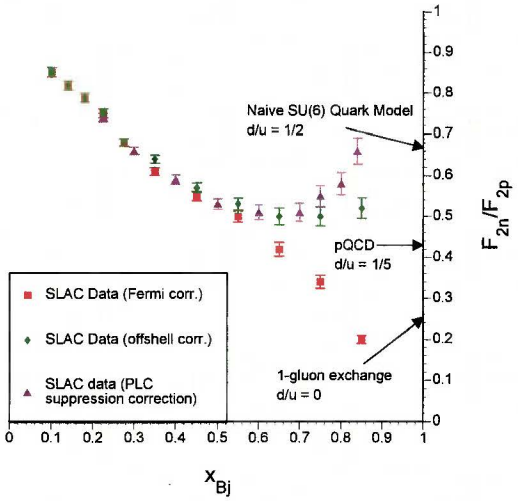

FIG. 16. [29] Neutron to proton structure function ratio, extracted from SLAC proton and deuteron data, assuming different nuclear corrections. Several theoretical predictions for the $x \to 1$ limits are indicated by arrows.

1. Predictions for d/u at Large x

Knowledge of PDFs is vital for the study of the flavor and spin dynamics of quarks inside the nucleon. The large x region is unique in allowing QCD predictions for PDFs in the limit of $x \to 1$, where a $1 - x$ expansion is possible.

In the SU(6) spin-flavor symmetric quark model, the wave function of a proton, polarized in the $+z$ direction for instance, would be simply

$$p\uparrow = \frac{1}{\sqrt{2}}u\uparrow(ud)_{S=0} + \frac{1}{\sqrt{18}}u\uparrow(ud)_{S=1} - \frac{1}{3}u\downarrow(ud)_{S=1} - \frac{1}{3}d\uparrow(uu)_{S=1} - \frac{\sqrt{2}}{3}d\downarrow(uu)_{S=1} \tag{A3}$$

where the subscript S denotes the total spin of the diquark partner of the quark. In DIS, exact SU(6) symmetry would be manifested in the same distributions for the valence quarks in the proton, which implies $d_v/u_v = 1/2$ for all x.

In nature, the nucleon N and Δ masses are different and the SU(6) symmetry is broken. Based on phenomenological [32] and Regge [33] arguments, the symmetry breaking can arise from the suppression of the $S = 1$ diquark configuration relative to the $S = 0$ diquark configuration, which leads to $d/u \to 0$ in the limit $x \to 1$ ($S = 0$ dominance). This expectation has been implicitly built into the PDF parameterizations utilized in most global

fits to parton distribution functions. The symmetry breaking can be understood within the one-gluon exchange quark model [34]. The color-magnetic hyperfine interaction between two quarks (i, j) is proportional to the dot product of their spins $\vec{S}_i \cdot \vec{S}_j$. This naturally leads to the mass splitting between N and Δ, and a softening of the d quark distribution relative to the u.

On the other hand, a perturbative QCD argument [35] shows that the exchange of longitudinal gluons would introduce a factor $(1-x)^{1/2}$ into the Compton amplitude relative to transverse gluon exchange. Thus the dominant reaction mechanism is DIS from a quark with the same spin orientation as the nucleon, i.e. spin projection of the diquark is zero, then $d/u \to 1/5$ as $x \to 1 (S_z = 0$ dominance). A similar result can be also obtained from the quark counting rules [36].

Experimental information on d/u at large x has mainly been constrained by charged lepton DIS scattering from the combination of the hydrogen and deuteron targets, with the typical analysis of deuteron data performed under the assumption that the deuteron is a system of two free nucleons moving with a Fermi momentum distribution. While the nuclear effects are expected to be small at small and intermediate x, the off-shell effects can significantly alter the extracted d/u ratio at large x, as shown in Figure 16 [29]. The off-shell correction can increase the d/u ratio, from $d/u \sim 0$ with $S = 0$ dominance to $d/u \sim 0.5$ with SU(6) symmetry and PLC (Point-Like Configurations) suppression correction.

2. Existing Neutrino and Anti-neutrino Data on d/u

The cross section for neutrinos on protons is sensitive to the d quark contribution. The d/u ratio can be obtained by combing the neutrino data and the charged lepton DIS data, for example by the Aachen-Bonne-CERN-Munich-Oxford collaboration in 1981 [37]. But the d/u can also be extracted from the neutrino and anti-neutrino cross section ratios in a single experiment, where some systematic uncertainties cancel.

For example, the WA21 experiment [38] measured the valence quark distribution with wide band neutrino and anti-neutrino beams, produced by 350 or 400 GeV protons from the CERN SPS, and the BEBC bubble chamber filled with liquid hydrogen, with fiducial volume of 19 m^3. The momenta of the final state muons were required to be greater then 4 GeV/c, while the neutrino energy was required to be between 20 GeV and 300 GeV, and

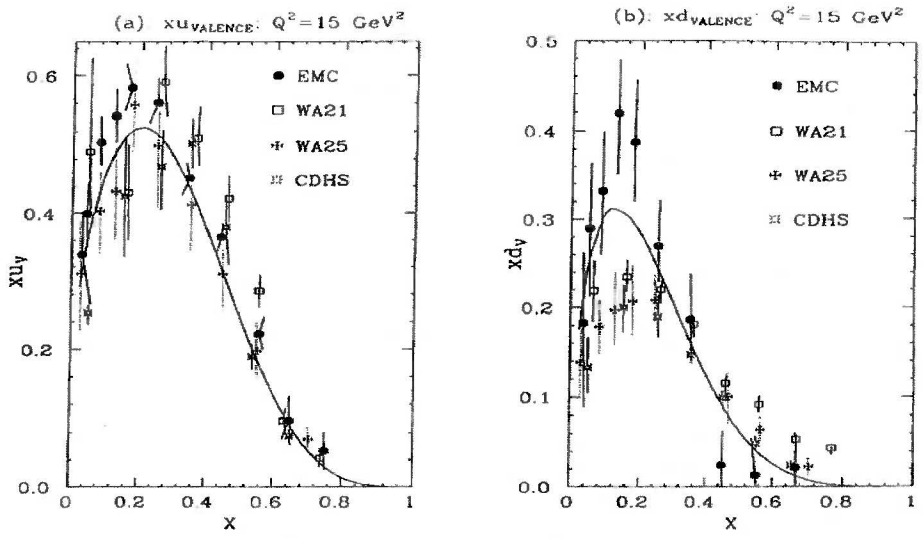

FIG. 17. [39] The x weighted valence quark distribution xu_v and xd_v as a function of x. The EMC data were taken with a muon beam. The WA21, WA25 and CDHS data were using neutrino and anti-neutrino beams on hydrogen, deuterium and iron targets respectively. The solid curve is a fit of Morfin and Tung.

Q^2 was required to be greater then 2 $(\mathrm{GeV/c})^2$ in order to suppress both the elastic and resonance backgrounds. After these cuts, 11800 νp and 7400 $\bar{\nu} p$ events were binned in x and y to extract the quark and anti-quark distributions. However, the WA21 data were not widely included in the global parameterization of PDFs, and one reason may be the distinct discrepancy in the shape of the xd_v quark distribution between the muon experiment (EMC) and the neutrino experiments with various targets (hydrogen in WA21,deuterium in WA25 and hydrogen in CDHS), as shown in Figure 17 [39].

3. Proposed Measurements on Hydrogen

As shown in Figure 18, the d/u ratio can be obtained directly from the neutrino to anti-neutrino cross section ratio on the hydrogen target, free of any nuclear correction and charge symmetry assumption. The acceptance of MINERνA detector for the CC events was considered in vertex reconstruction, which requires another charged trackable particle in the MINERνA detector in addition to the muon. The muons have to reach the upstream end of

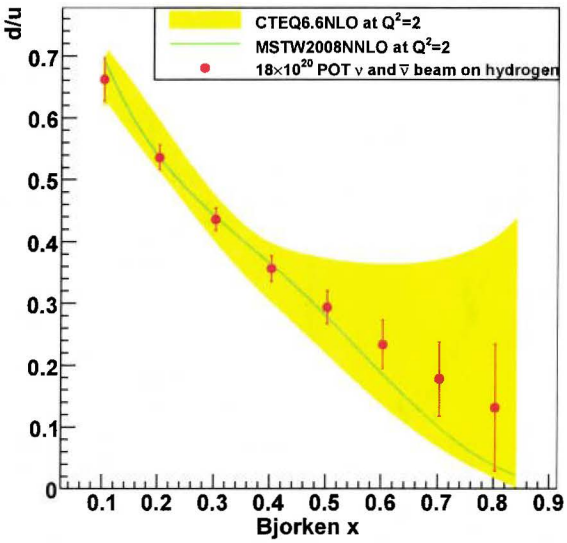

FIG. 18. The projected d/u ratio measurement on a hydrogen target, as well as the global parameterizations of d/u from MSTW08 and CTEQ6.6 at $Q^2 = 2$ GeV^2. The uncertainties were estimated assuming $d/u = (1-y)^2\sigma^{\nu p}/\sigma^{\bar{\nu}p}$, which is only valid at large x with negligible sea quark contributions.

the MINOS detector or stop inside the MINERνA detector. The empty target subtraction uncertainty was also included assuming an optimum running time. As shown in Figure 19, the CSV can be also extracted by combining the proton data with the world charged lepton data, which provides a neutron to proton structure function ratio. Both figures 18 and 19 assume a run of 18×10^{20} protons on target in each of the neutrino and anti-neutrino beams in the NuMI Medium Energy beam.

Appendix B: Safety Concerns for Cryogenic Hydrogen/Deuterium

Cryogenic targets have been used widely at Fermilab. Ten out of the fourteen fixed target beam lines of Tevatron had experiments with a cryogenic system. One of the first and largest cryogenic systems ever operated at Fermilab was the 15 ft hydrogen bubble chamber, which held 30 m^3 liquid hydrogen. The system operated for 15 years without a serious safety incident.

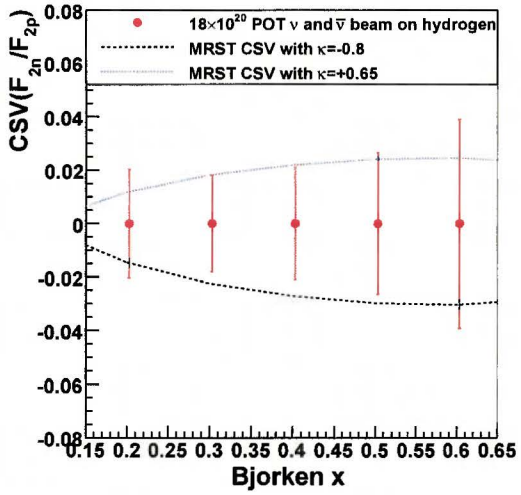

FIG. 19. The projected sensitivity in hydrogen to the charge symmetry violation in terms of $CSV(F_{2n}/F_{2p}) = \frac{F_{2n}}{F_{2p}} - \frac{4d_p+u_p}{4u_p+d_p}$ as a function of Bjorken x, based on the comparison of the proposed hydrogen measurement. The uncertainty contributions from the sea quark distributions and charged lepton data were ignored. The 90% confidence level limit for CSV from MRST was also plotted, with $-0.8 \leq \kappa \leq +0.65$.

Specific fire hazard and cryogenic concerns will need to be addressed to repurpose the existing cryogenic helium target. Likely upgrades required to operate fill the cryostat with hydrogen or deuterium include improvements to the existing ventillation piping to the surface and a secondary containment volume around the target. If interest in the physics goals of this proposal is sufficient, we would proceed with an engineering study to look at possible approaches and costs.

[1] D. F. Geesaman, K. Saito, and A. W. Thomas, Annu. Rev. Nucl. Part. Sci **45**, 337-390 (1995).

[2] J. Seely *et al.*,Phys. Rev. Lett. **103**, 202301 (2009).

[3] D. M. Alde *et al.* [FNAL-772 experiment] Phys. Rev. Lett. **64**, 2479 (1990).

[4] A. M. Cooper *et al.* [WA25 and WA59 Collaboration], Phys. Lett. B **141**, 133 (1984).

[5] J. Guy *et al.* [WA25 and WA59 Collaboration], Z. Phys. C **36**, 337 (1987).

[6] M. Tzanov *et al.*, Phys. Rev. D **74**, 012008 (2006).

[7] J. F. Owens *et al.*, Phys. Rev. D **75**, 054030 (2007).

[8] I. Schienbein *et al.*, Phys. Rev. D **80**, 094004 (2009); Phys. Rev. D **77**, 054013 (2008).

[9] MINERνA (Main INjector ExpeRiment ν-A), FNAL-E-0938, proposed in 2003, arXiv:hep-ex/0405002; http://minerva.fnal.gov/.

[10] Elliot Leader and Enrico Predazzi, *An introduction to gauge theories and modern particle physics*, Cambridge University Press (1996).

[11] J. Gomez *et al.*, Phys. Rev. D **49**, 4348 (1994).

[12] J. Arrington, J. Phys. Conf. Ser.**69**, 012024 (2007) [arXiv:nucl-ex/0701017].

[13] S. A. Kulagin and R. Petti, Phys. Rev. D **76**, 094023 (2007).

[14] J. T. Londergan and A. W. Thomas, J. Phys. G **31**, 1151 (2005).

[15] J. T. Londergan, J. C. Peng and A. W. Thomas, Rev. Mod. Phys. **82**, 2009 (2009).

[16] B.-Q. Ma, Phys. Lett. B **274**, 111 (1992).

[17] B.-Q. Ma, A. Schäfer and W. Greiner, Phys. Rev. D **47**, 51 (1993).

[18] E. Sather, Phys. Lett. B **274**, 433 (1992).

[19] G. P. Zeller *et al.* [NuTeV Collaboration], Phys. Rev. D **65**, 111103 (2002).

[20] E. N. Rodionov, A. W. Thomas and J. T. Londergan, Mod. Phys. Lett. **A9**, 1799 (1994).

[21] A. D. Martin, R. G. Roberts, W. J. Stirling, and R. S. Thorne, Eur. Phys. J. C **35**, 325 (2004).

[22] JLab experiment E09-002, *Precise Measurement of π^+/π^- Ratios in Semi-inclusive Deep Inelastic Part I: Charge Symmetry Violating Quark Distributions*, Spokersperson: K. Hafidi (contact person), D. Gaskell, D. Dutta.

[23] M. Paolone *et al.*, Phys. Rev. Lett. **105**, 072001 (2011); S. P. Malace *et al.*, Phys. Rev. Lett. **106**, 052501 (2011).

[24] NOνA (Numi Off-axis ν Appearance experiment), FNAL-P-0929, proposed in 2004;

http://wwwnova.fnal.gov/.

[25] MINOS (Main Injector Neutrino Oscillation Search), FNAL-E-0875, proposed in 1995; http://wwwnumi.fnal.gov/.

[26] http://projects.hepforge.org/genie/.

[27] P. M. Nadolsky *et al.*, arXiv:0802.0007.

[28] A. D. Martin, W. J. Stirling, R. S. Thorne and A. D. Martin, Eur. Phys. J. C **63**, 189 (2009).

[29] JLab BONUS experiment, E-03-012, *The Structure of the Free Neutron Via Spectator Tagging.* Co-spokerspersons: H. Fenker, C. E. Keppel, S. Kuhn (contact person) and W. Melnitchouk.

[30] JLab 12 GeV BONUS proposal, E12-10-102 (update of E12-06-113), *The structure of the free neutron at large x-Bjorken.* Co-spokerspersons: S. Büeltmann (contact person),S. E. Kuhn, M. E. Christy, C. E. Keppel, H. Fenker, W. Melnitchouk, and K. Griffioen.

[31] JLab 12 GeV MARATHON proposal, E12-10-103 (update of E12-06-118), **M***e***A***surement of the* F_2^n/F_2^p*, d/u* **RA***tios and A=3 EMC Effect in Deep Inelastic Electron Scattering off the* **T***ritium and* **H***elium Mirr***O***r* **N***uclei.* Co-spokerspersons: G. G. Petratos (contact person), J. Gomez, R. Holt, and R. Ransome.

[32] F. E. Close, Phys. Lett. B **43**, 422 (1973).

[33] F. E. Carlitz, Phys. Lett. B **58**, 345 (1975).

[34] N. Isgur, Phys. Rev. D **59**, 034013 (1999).

[35] G. R. Farrar and D. R. Jackson, Phys. Rev. Lett. **35**, 1416 (1975).

[36] S. J. Brodsky, M. Burkardt and I. Schmidt, Nucl. Phys. B **441**, 197 (1995).

[37] P. Allen *et al.* [Aachen-Bonn-CERN-Munich-Oxford Collaboration], Phys. Lett. B **103**, 71 (1981).

[38] G. T. Jones *et al.* [WA21],Z. Phys. C **44**, 379 (1989).

[39] G. Sterman *et al.*, *Handbook of perturbative QCD*, Rev. Mod. Phys. **67**, 157 (1995).

[40] Fermilab Environment, Safety and Health Handbook, internal document, Fermilab ES&H Section, revised in 2006.